Enhanced photoresponse of Ge/Si nanostructures by combining amorphous silicon deposition and annealing

A. Podolian,[1] A. Nadtochiy,[1] O. Korotchenkov,[1,a)] B. Romanyuk,[2] V. Melnik,[2] and V. Popov[2]

[1]*Department of Physics, Taras Shevchenko Kyiv National University, Kyiv 01601, Ukraine*
[2]*V. Lashkarev Institute of Semiconductor Physics NAS of Ukraine, Kyiv 03028, Ukraine*

In order to inhibit high carrier recombination rates in Ge-on-Si nanostructures, Ge_xSi_{1-x} nanoislands were covered by a thin amorphous silicon layer *via* a low pressure CVD process. It is demonstrated that the surface photovoltage (SPV) signal in capped Ge_xSi_{1-x}/Si is increased by an order of magnitude compared to that of bare Ge_xSi_{1-x} islands, which can be due to the effective passivation of recombination centers at the a-Si/Ge_xSi_{1-x} interface. The effect is even more enhanced after subsequent annealing at $400\,^\circ$C in an O_2 ambient environment, with the signal increases ranging from 5 to 10 times. The observed increased photovoltage is accompanied by longer time decays in the SPV transients, being most increased after the annealing step. These results show that the photoexcited electron-hole pairs can be efficiently separated by the internal electric field at the a-Si/Ge_xSi_{1-x}/c-Si interfaces and can contribute to the photovoltage with decreasing recombination in Ge_xSi_{1-x} islands or at the interfaces. This work can facilitate the photovoltaic applications of Ge/Si heterostructures. *Published by AIP Publishing.*
https://doi.org/10.1063/1.5029948

I. INTRODUCTION

Incorporating a small bandgap Ge_xSi_{1-x} layer, capable of absorbing more in the longer wavelengths of the solar spectrum, is attractive for increasing the overall photocurrent and efficiency of thin-film crystalline Si (c-Si) solar cells and photodetectors.[1–5] In order to avoid the lattice defect formation occurring upon relaxation of a SiGe-layer with a thickness larger than the critical thickness,[6] Ge layers can be grown to form three-dimensional islands or quantum dots in the Stranski-Krastanov growth mode.[7] Both increased response in the infrared and overall performance increase have been achieved with this approach,[8] which is of crucial importance for photovoltaic and electronic applications. These applications require embedded Ge_xSi_{1-x} species having very low defect densities and excellent optical and electronic properties.

In the c-Si material, the discontinuity of the crystal arrangement at the surface creates the dangling bonds, which act as good recombination centers and decrease the carrier lifetime.[9] To improve the efficiency for absorbing light and operating lifetime, the front surface of the solar cell normally consists of well-passivated antireflective coating of thermal SiO_2 or Si_3N_4 layers.[10,11]

In another approach, the amorphous silicon (a-Si) layers can be used as a top surface passivation coating for c-Si.[12–18] It has been reported that a-Si/c-Si heterostructures are advantageous with respect to enlarged separation lengths for photogenerated charge carriers,[19] as the desired minority carriers can be repelled from the interface, which reduces the recombination at the Si surface.

Quite recently, a-Si/c-Ge_xSi_{1-x}/c-Si heterojunction solar cells have been proposed, which offer efficiencies superior to SiGe-based thin film solar cells.[20] It has been reported that placing a passivating a-Si:H thin layer on the front side of the n–$Si_{0.85}Ge_{0.15}$/p–c-Si heterojunction solar cell can passivate the front surface, which reduces the carrier recombination velocity at the front contact of the solar cell and increases the cell efficiency.[21] Electron transport by hopping conduction in terms of the carrier activation hopping over energy barriers has been observed in a-Si/c-Ge_xSi_{1-x}/p–c-Si thin films although a thorough understanding of the conduction mechanism in these materials would be essential for their application in solar cells.[22]

However, there have been surprisingly a small number of studies concerned with the surface photovoltage (SPV) measurements and SPV decay times in a-Si/Ge_xSi_{1-x}/c-Si systems, which are of crucial importance for the design of photovoltaic, electronic, and optoelectronic devices.

In this work, we demonstrate that the SPV signal can be enhanced due to capping of Ge_xSi_{1-x} islands on Si with a-Si and after a subsequent annealing at $400\,^\circ$C in an O_2 ambient atmosphere. The observed enhancement is accompanied by longer time decays in the SPV transients. These results can be applied for optimizing the Si/Ge layer design in thin film solar cells.

II. EXPERIMENTAL

To grow Ge_xSi_{1-x} on Si, electronic grade 300-μm thick p-type Cz-Si(100) wafers with a mirror surface on the front side and chemical polishing on the back side were used. Their resistivity was 10 Ωcm, and approximate bulk lifetime measured from the photocurrent decay was about 700 μs. First, an ex-situ standard RCA cleaning process with HF dip

a)Electronic mail: olegk@univ.kiev.ua

last treatment and a H_2 prebake at $1000\,°C$ to remove native oxide were carried out. Without exposing the wafer to air, a 5 nm thick masking chemical vapor deposition (CVD) oxide was grown on the cleaned substrate. Here, an ultra-thin, porous SiO_2 layer was used to achieve an epitaxial growth of germanium nano-dots with densities exceeding $10^{12}\,cm^{-2}$ through existing nano-windows.[23]

The Ge deposition was performed in the reduced pressure CVD system under the same process conditions as described elsewhere.[24,25] The initial Ge seed layer was grown at $300\,°C$ using a N_2-GeH_4 gas mixture. Then, the wafer was heated up to $550\,°C$ in H_2 and the Ge growth was continued with a H_2-GeH_4 gas mixture, resulting in a 7 monolayer thick ($\approx 2.3\,nm$) Ge_xSi_{1-x} layer (referred to later as sample set G).

In a strained Ge_xSi_{1-x} layer grown on Si, isolated islands can be formed, as described in detail elsewhere.[26,27] These islands were characterized using a scanning probe atomic force microscope (AFM) NanoScope IIIa. The resulting images are exemplified in Fig. 1.

These samples were subsequently surface-coated with 10-nm thick a-Si layers by low pressure CVD (referred to as sample set G_2). This was done by using the thermal decomposition of silane, $SiH_4 = Si + 2H_2$, at $520\,°C$.[28] To study the influence of the thermal treatment, the G_2 samples were additionally furnace annealed for 5 minutes at $400\,°C$ in an O_2 ambient atmosphere (sample set G_2^1).

SPV transients were measured in the capacitor arrangement using a red light-emitting diode (LED) with a pulse width of 100 ns as an excitation source. Details of our setup are given elsewhere.[29] A parallel plate capacitance was formed between a metal grid electrode with a transparency of $\leq 30\%$ and the structure, separated by a mica insulating foil with a thickness of about $20\,\mu m$. A 1-$G\Omega$ load resistor, a high-impedance buffer cascade (input resistance $10^{13}\,\Omega$, output resistance $50\,\Omega$) based on a field-effect transistor, and a sampling digital oscilloscope were used in the measurements. The measuring circuit was carefully screened to ensure that the experimental system was not susceptible to electronic pickups or ground loop effects. The scanning SPV apparatus, which provides wafer maps of both the SPV magnitude and decay time with a 100-μm spatial resolution, was
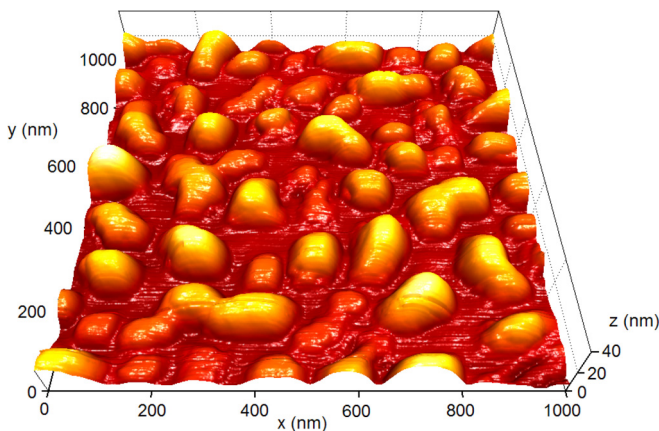
discussed elsewhere.[30] The scanning area for each sample was $4\,mm \times 7\,mm$.

Raman spectra were collected at room temperature using a Horiba Jobin-Yvon T-64000 Raman spectrometer equipped with a TE-cooled CCD detector. The 488.0 nm line of the Ar^+/Kr^+ laser was used for excitation. Measurements were performed in the $z(x,y)\bar{z}$ scattering geometry, where x, y, and z correspond to the crystallographic directions [100], [010], and [001] of Si, respectively.

III. RESULTS AND DISCUSSION

While Ge island alloying during deposition takes place at the interface with the Si substrate, the Si removed from the substrate diffuses into the growing islands, resulting in Ge-rich Ge_xSi_{1-x} islands in sample G. When the samples are capped with a 10 nm a-Si layer (samples G_2 and G_2^1), the Si interdiffusion from the capping layer may occur, which may lead to a further increase in the Si content in the islands. Here, we address this issue by using Raman scattering to analyze the optical phonon region and extract the average Ge content x in the Ge_xSi_{1-x} islands.

Figure 2 shows Raman spectra of our samples. There are two distinct peaks centered near $\omega_1 \approx 300\,cm^{-1}$ and $\omega_2 \approx 405\,cm^{-1}$, which are due to the scattering from optic phonons involving Ge-Ge and Si-Ge vibrations, respectively.[31] It is seen that their frequencies, ω_1 and ω_2, slightly vary in different sample sets (see Table I), indicative of varying average strain and composition in Ge_xSi_{1-x}.

The frequencies of the two modes can be fitted *via* varying the Ge fraction x and strain as follows:[32]

$$\omega_1 = 284 + 5x + 12x^2 + b_1\langle S_\parallel \rangle, \quad (1)$$

$$\omega_2 = 400 + 29x - 95x^2 + 213x^3 - 170x^4 + b_2\langle S_\parallel \rangle, \quad (2)$$

where $\langle S_\parallel \rangle$ is the average in-plane strain, $b_1 = -400\,cm^{-1}$ is the phonon strain-shift coefficient for the Ge-Ge mode, and $b_2 = -575\,cm^{-1}$ is that for the Si-Ge mode.[31,33] This calculation yields the x and $\langle S_\parallel \rangle$ values, which are given in Table I.

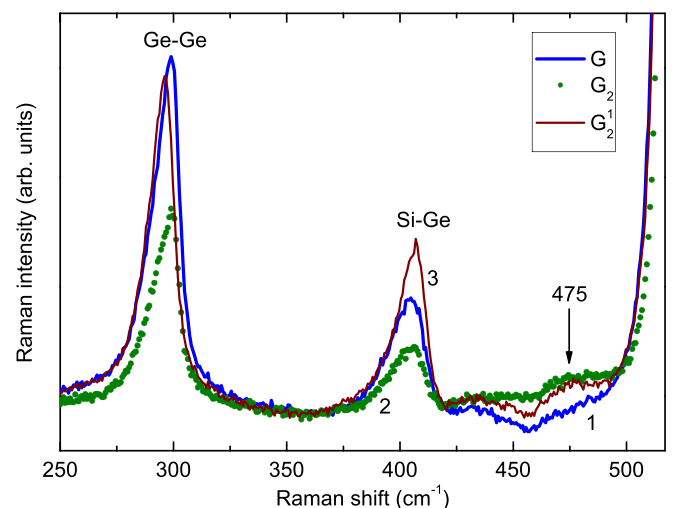
FIG. 1. AFM image of the surface of sample G.

FIG. 2. Raman spectra of samples G (1), G_2 (2), and G_2^1 (3).

TABLE I. Frequencies of the Raman modes and calculated values of x and $\langle S_\parallel \rangle$.

Sample	ω_1 (cm^{-1})	ω_2 (cm^{-1})	x	$\langle S_\parallel \rangle$ (%)
G	298.9	404.6	0.818	−0.69
G_2	299.1	405.0	0.817	−0.75
G_2^1	296.0	406.3	0.753	−0.36

It is seen that the concentration of Ge atoms in the Ge_xSi_{1-x} islands is about 82% for sample G. After capping with a 10 nm a-Si layer in sample G_2 the Ge content is preserved, whereas subsequent annealing at 400 °C in an O_2 ambient atmosphere decreases the Ge fraction down to about 75%.

It is well known that the surface photovoltage monitors the excess carrier density adjacent to the surface.[34] If we consider long enough light pulse widths, greater than the carrier lifetime τ, the penetration depth of the minority carriers is of the order of the minority carrier diffusion length L, which is related to τ as $L = \sqrt{D\tau}$ with D the diffusion coefficient. Furthermore, if the recombination lifetime in the near-surface space charge region is greater than the recombination lifetime in the bulk, the surface density of excess carriers decays with the same time constant as carriers elsewhere in the sample.

In our case, the light pulse width was chosen to be much smaller than τ. As shown by Luke and Cheng,[35] the minority-carrier profile below the surface is determined by $1/\alpha$ ($\approx 3\,\mu m$ at the light absorption coefficient $\alpha = 3.1 \times 10^3\,cm^{-1}$ in c-Si[36]) rather than by the diffusion length L. Therefore, the SPV decay is determined mostly by the recombination lifetime in the space charge region, and the observed changes in the SPV decay times and magnitudes are primarily related to the near-surface recombination processes modified by the deposition of a-Si and subsequent annealing.

Figure 3 shows SPV decays obtained in our samples. They are taken by averaging over the light beam diameter of
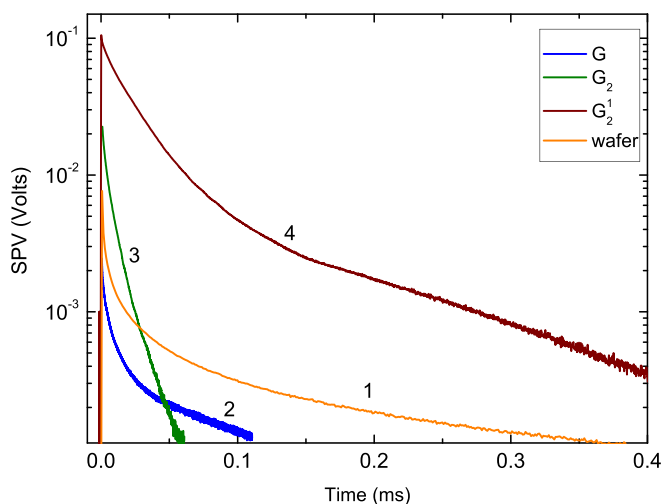

FIG. 3. Time-dependent SPV of Si wafer (1), samples G (2), G_2 (3), and G_2^1 (4). The decays are taken with unfocused 640-nm LED light striking the sample surface, about 5 mm in diameter.

about 5 mm in order to reproduce the behavior of a solar cell capable of converting unfocused solar energy into electricity. It is seen that most of the decays are non-exponential, as, seemingly, only curve 3 more closely resembles the single exponent.

The most prominent effect in Fig. 3 is the SPV enhancement due to capping sample G with a-Si (curves 3 and 4 compared with curves 1 and 2 at time $t = 0$). It is seen that the SPV magnitude is increased by an order of magnitude in the capped Ge_xSi_{1-x}/Si (curve 3 at time $t = 0$) compared to that of bare Ge_xSi_{1-x} islands (curve 2), and the effect is even more enhanced after subsequent annealing in an O_2 ambient atmosphere, ranging from about 5 to 10 times increase (curve 4 at time $t = 0$).

A recent survey of most common models used to describe carrier decay processes is given by Gaubas *et al.*[37] For example, a simple double-exponential carrier decay transient can be observed due to carrier trapping. At low excess carrier densities, the solution of the rate equations for free carriers and those trapped on shallow levels leads to the effective excess carrier decay lifetime of recombination with trapping, which is determined by three partial lifetimes of recombination through deep levels, carrier trapping at shallow levels, and thermal release from shallow levels.

However, we anticipate that the behavior of photoexcited charge carriers at the surface shown in Fig. 1 can be better described by multi-trapping of charge carriers in disordered systems. It is known that disordered structures of different types lead to more complicated carrier decay transients, which are often due to trapping-limited diffusion in randomly distributed sinks.[38–40] It is quite evident that the observed SPV decay can be viewed as due to recombination not only through centers in the islands and a-Si layer but also through states at the Ge_xSi_{1-x}/SiO_2 and a-Si/Ge_xSi_{1-x} interfaces. It is important to note that, in the case of a distribution of decay times, e.g., due to a distribution of the energies of these states and of the dynamics of carrier capture and emission, non-exponential decay characteristics may be obtained. Then, for various distributions of the decay times, the resulting behavior yields various temporal dependencies of the SPV.

Such a decay time distribution can be described by a stretched-exponential decay model,[41] so that the decay curves given in Fig. 3 were fitted to a stretched-exponential time decay,

$$U(t) = U_0 e^{-(t/\tau_0)^\beta}, \qquad (3)$$

with the characteristic stretched-exponent decay time τ_0 and the dispersion factor β, which describes the spread of time constants. Thus, $\beta = 1$ for a monoexponential decay, while a stretching parameter $0 < \beta < 1$ describes a variation from a monoexponential transient such that the smaller value of β corresponds to the broader distribution of decay times.

More detailed information can be derived by analyzing the spatially distributed τ_0 and β, which are shown in Figs. 4 and 5. The maps give spatially inhomogeneous τ_0 and β, which are most likely a consequence of the fabrication
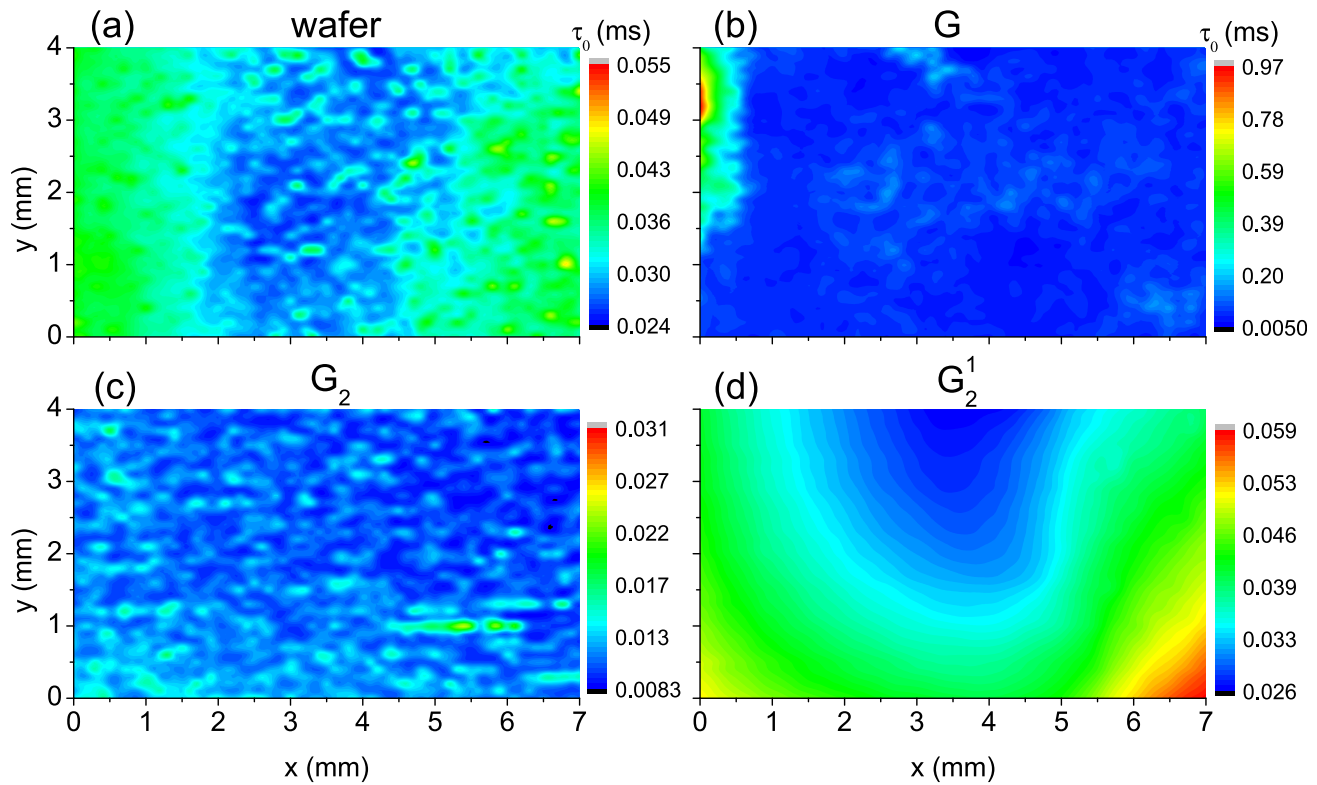
FIG. 4. Maps of the surface distribution of τ_0 in Si wafer (a), samples G (b), G_2 (c), and G_2^1 (d). The decays are taken with a LED light focused to a spot of $100\,\mu m$ in diameter.

process and treatment steps, although quantitative conclusions are hardly feasible. Nevertheless, the general result is that the values of τ_0 and β are markedly non-uniform after capping with a 10 nm a-Si layer in sample G_2, as evidenced by images (c) in Figs. 4 and 5. Images (d) in Figs. 4 and 5 show much more homogeneous distribution of τ_0 and β, as ripple patterns most clearly seen in Figs. 4(c) and 5(c) are remarkably obscured.
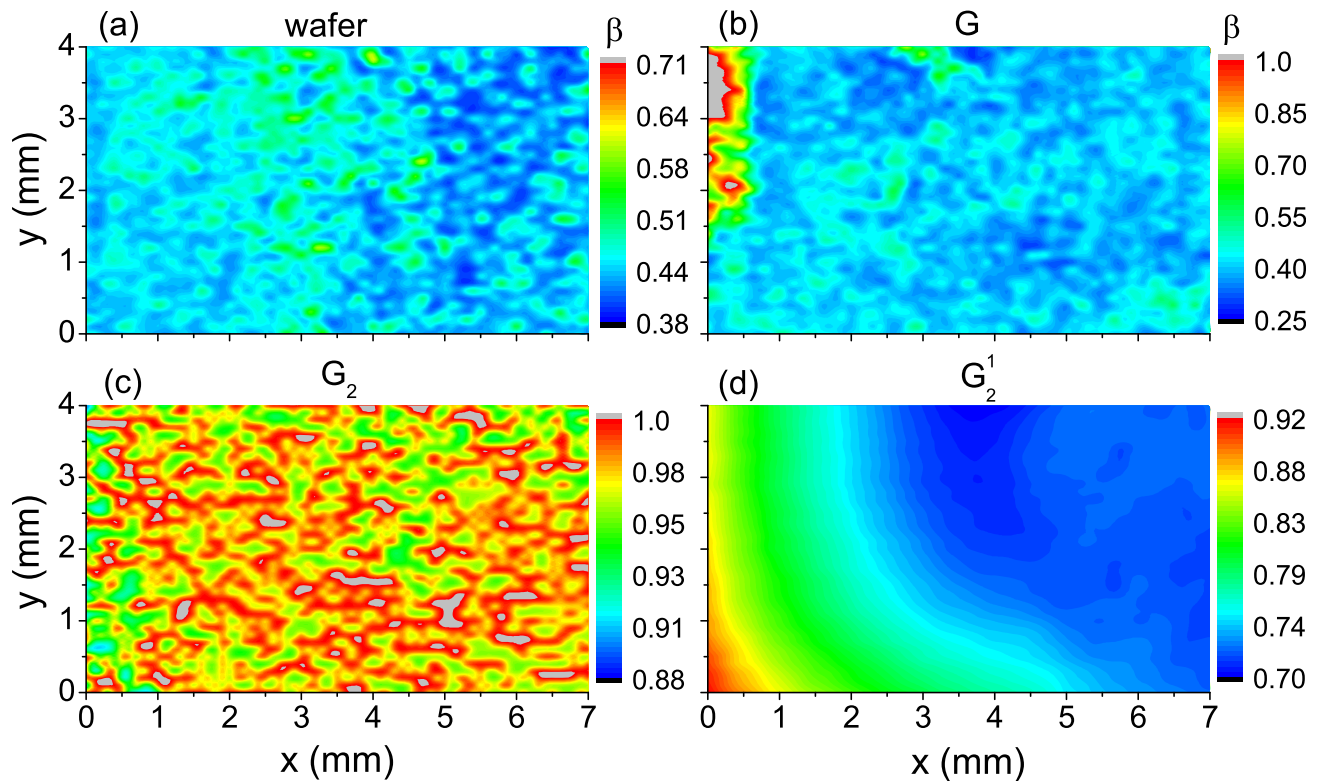

FIG. 5. Maps of the surface distribution of β in Si wafer (a), samples G (b), G_2 (c), and G_2^1 (d). The decays are taken with a LED light focused to a spot of $100\,\mu m$ in diameter.

By statistically analyzing the images shown in Figs. 4 and 5, we compute the probabilities to find particular values of U_0, τ_0, and β in Eq. (3), which allow drawing useful conclusions about the surface-distributed SPV decay times and the effect of passivating the interface states at the surface of the Ge_xSi_{1-x} islands and at the buried interfaces.

The values of U_0 and characteristic time constants τ_0 for all our samples are plotted in Fig. 6, whereas the values of the β factor are shown in Fig. 7. For comparison, we also show the U_0, τ_0, and β distributions reproduced in the Si wafer, which served as a freshly prepared substrate for growing our nanostructures; see Figs. 6(a) and 7(a).

The main effects are clearly revealed in Figs. 6(a) and 6(b). Depositing a porous SiO_2 layer and, subsequently, Ge_xSi_{1-x} islands (sample G) quenches the SPV signal making it noticeably broader, as shown in Figs. 6(a) and 6(b). The τ_0 distribution becomes significantly narrower, as evidenced by insets in Figs. 6(a) and 6(b). A rather complicated interface structure in our Ge_xSi_{1-x}-on-Si sample yields that the measured decay times are non-uniformly distributed across the wafer surface, so that much longer τ_0, up to ≈ 1 ms, can be realized in sample G, as seen in the inset of Fig. 6(b) and in Fig. 4(b).

Another important clue can be observed in Fig. 7. While the β distribution peak for sample G decreases in intensity
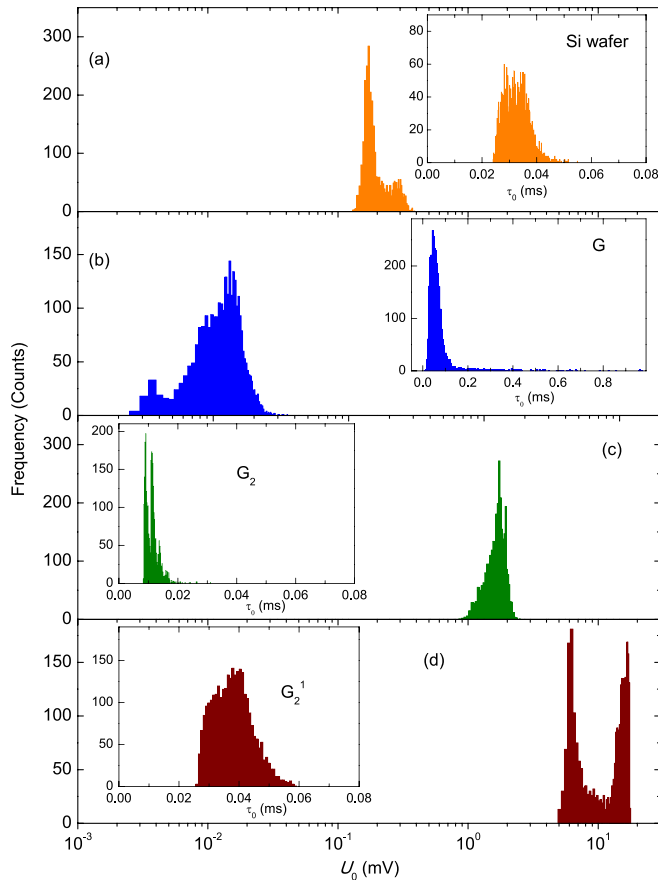

FIG. 7. Probability of occurrences of a particular value of β in Si wafer (a), samples G (b), G_2 (c), and G_2^1 (d). The measurement conditions are similar to those in Fig. 6.

and slightly shifts to smaller values in Fig. 7(b) compared to that in the wafer given in panel (a), some of the carrier decay channels in sample G produce a monoexponential decay with $\beta = 1$, which can thus be viewed as being nearly contained within a perfect Ge_xSi_{1-x}/Si interface.[42]

This effect is even more pronounced after the Ge_xSi_{1-x} islands were coated with amorphous silicon in sample G_2, as seen in Fig. 7(c). The β distribution peak is drastically suppressed with the peak position shifted towards $\beta = 1$. Gaining the strength, as evidenced by increased U_0 in Fig. 6(c), the SPV signal decays nearly monoexponentially [strong peak at $\beta = 1$ in Fig. 7(c)], which is also seen in curve 3 of Fig. 3 exhibiting the monoexponential decay.

We can attempt to understand the effect by taking into account that hydrogenated amorphous silicon films have outstanding passivation effects in crystalline silicon surfaces, and insertion of an ultrathin SiO_x layer at the a-Si:H/c-Si interface has significant influences on the passivation effect.[43] The SiO_x layer serves as a barrier to prevent the epitaxial growth of a-Si:H at a nonsharp a-Si:H/c-Si interface, thus improving the quality of the a-Si:H/c-Si interface.

In order to clarify the likely involvement of the SiO_x species, an additional annealing step at 400 °C in an O_2 ambient atmosphere (sample G_2^1) was done. After our samples were annealed at 400 °C, both the SPV magnitude U_0 and the decay time τ_0 remarkably increase, spreading out over greater intervals; see Fig. 6(d). The contribution of the

FIG. 6. Probability of occurrences of a particular values of U_0 and τ_0 (insets) in Si wafer (a), samples G (b), G_2 (c) and G_2^1 (d), which are measured by surface mappings of the SPV decays. The values of U_0 and τ_0 are obtained by fitting all the surface-collected decays to a stretched-exponential form. The decays are taken with a LED light focused to a spot of 100 μm in diameter.
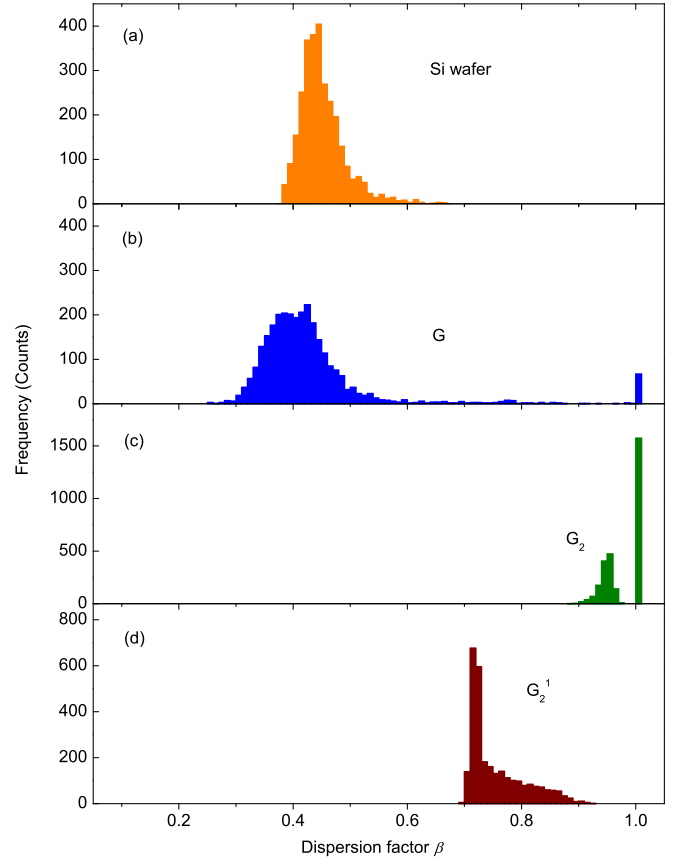
monoexponential decays drops at the expense of the strong peak at about $\beta = 0.7$, as shown in Fig. 7(d). An increase in the SPV signal taken in sample G_2^1 is accompanied by longer time decays in the SPV transients [(d) in Fig. 6] over those for samples G and G_2 [(b) and (c) in Fig. 6, respectively].

Based on the above derivations, we now consider a schematic sketch of the Ge_xSi_{1-x} islands and the buried interfaces (see Fig. 8) that can explain the observed SPV results. We suggest that the strain, which arises in the growing Ge_xSi_{1-x} layer at the Ge_xSi_{1-x}/SiO_2 interface ($\langle S_\| \rangle$ in Table I), worsens the quality of the a-Si:H/Ge_xSi_{1-x} interface. This creates micro void regions with dangling and floating bonds in the island/surrounding matrix environment, which form randomly distributed sinks acting as undesirable recombination centres. The annealing step at 400 °C in an O_2 ambient atmosphere done in sample G_2^1 allows for a partial strain relaxation, as supported by the Raman data given in Table I ($\langle S_\| \rangle = -0.36\%$ in sample G_2^1 compared with $\langle S_\| \rangle = -0.75\%$ in sample G_2). This annealing may oxidize a-Si and form the above SiO_x species thus improving the quality of the Ge_xSi_{1-x}/SiO_2 interface.

The second important feature is related to the direct saturation of the surface dangling bonds shown in Fig. 8 by the oxygen passivating particles that diffuse into the island/surrounding matrix environment. Third, the Ge_xSi_{1-x}/Si interface quality is improved due to the passivation by H. Hydrogen diffusion occurs laterally across the Ge_xSi_{1-x} and SiO_2 surfaces and beneath the a-Si:H thin layer by localized hopping,[44] where the hydrogen absorbed at one site jumps to another site *via* shallow trapping states. Reaching the Ge_xSi_{1-x}/Si interface, hydrogen passivates the interface defects, which in turn improves the interface quality and enhances the photoresponse.

Therefore, these results show that the photoexcited electron-hole pairs are efficiently separated at the a-Si/Ge_xSi_{1-x}/c-Si interfaces contributing to SPV with decreasing recombination in the island/surrounding matrix. The recombination time can be defined as $\tau_r = \Delta n / R$, where Δn is the excess carrier density and R is the recombination rate. Then, the SPV signal magnitude is $U_0 = (e\Delta n/\varepsilon\varepsilon_0)L$, where ε is the dielectric function, ε_0 is the permittivity of free space, e is the elementary charge, and L is the charge separation length. This yields

$$U_0 = \frac{e\tau_r RL}{\varepsilon\varepsilon_0},\qquad(4)$$

expressing the trend that increasing U_0 would increase τ_r and thus prolong the SPV decay times, which is indeed the case in Fig. 3.

It has been shown that crystallization of a-Si:H may occur at the temperatures employed in this work.[45–48] In order to address this issue, Raman spectra of the sample surface in the range from ≈440 to $600\,cm^{-1}$ were analyzed in greater detail (see Fig. 9). An extra scattering in the range from 460 to $490\,cm^{-1}$ observed in samples G_2 and G_2^1 capped with a-Si (arrow in Fig. 2) appears as a result of effective density of transverse optical (TO) vibration modes in a-Si:H,[49] and thus, it can be attributed to the amorphous silicon phase.

The analysis of the spectra shown in Fig. 9 followed a three-peak fitting centered at $\approx520\,cm^{-1}$, $500 \pm 10\,cm^{-1}$, and $480 \pm 10\,cm^{-1}$, corresponding to the TO phonon of c-Si, defective part of the crystalline phase or a fine crystalline phase in the layer,[50–53] and amorphous contributions, respectively (solid lines in Fig. 9). The crystallinity factor was calculated by $f_c = (I_{500} + I_{520})/(I_{500} + I_{520} + 0.8I_{480})$,[54] where
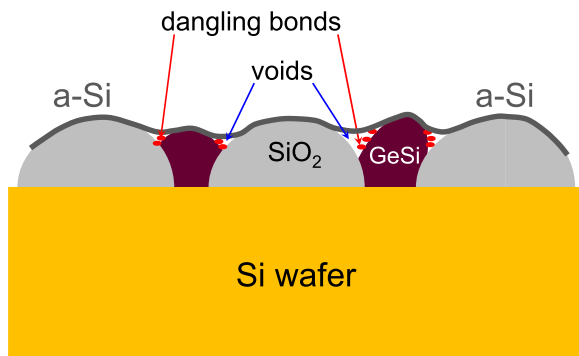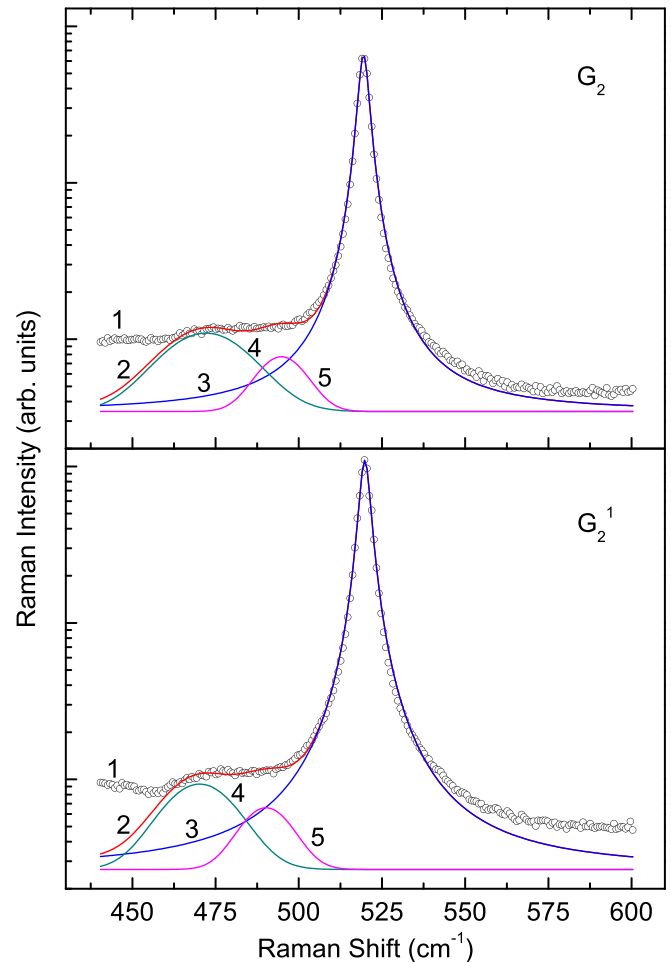

FIG. 8. Schematics of the a-Si/Ge_xSi_{1-x}/Si structure illustrating the Si substrate, porous SiO_2, GeSi islands, and a-Si layer with dangling bonds at the island surface in micro voids.

FIG. 9. Raman spectra (curves 1) of samples G_2 and G_2^1 (portions of spectra 2 and 3 in Fig. 2 enlarged in the range from 440 to $600\,cm^{-1}$). The data fits (curves 2) consist of the sums of a Lorentzian peak function at $520\,cm^{-1}$ (curves 3) and Gaussian peak functions at 480 ± 10 (curves 4) and $500 \pm 10\,cm^{-1}$ (curves 5).

I is the area of each respective peak. We got $f_c = 0.99$ in sample G, 0.95 in sample G_2, and 0.98 in sample G_2^1.

It is apparent that capping with a-Si decreases f_c in sample G_2 due to a thin amorphous layer. Sample G_2^1 has less a-Si content than sample G_2 but still less crystal fraction than sample G due probably to microcrystallization, which occurs after annealing at 400 °C.

It was also reported that atomic and molecular chains possessing micro voids would affect the density of localized states, which act as efficient recombination centers.[55] It turns out that there may be ways to reduce the density of states by increasing the annealing temperature, which is accompanied by orders of magnitude increase in the recombination lifetime of the majority carriers.[56] Therefore, a segregation of hydrogen atoms around the voids, which are organized in coordinated networks and reorganized during annealing,[57–59] may hence explain part of the experimental results on τ_0 (see Fig. 3), discussed earlier.

IV. CONCLUSIONS

In summary, we report the enhanced photovoltage in Ge_xSi_{1-x}-on-Si nanostructures after their capping with a thin amorphous silicon layer and a subsequent annealing at 400 °C in an O_2 ambient atmosphere. It is found that the surface photovoltage can be enhanced by up to 10 times as compared with the SPV signal observed in unannealed samples, which provides an excellent opportunity for solar cell applications. The increase in the SPV magnitude is accompanied by a prolonged SPV decay time, being greatly increased after the annealing step. These results can be used to engineer silicon-germanium based photovoltaic materials with high efficiency.

[1]K. Said, J. Poortmans, M. Caymax, R. Loo, A. Daami, G. Bremond, O. Kruger, and M. Kittler, Thin Solid Films **337**, 85 (1999).
[2]G. Beaucarne, F. Duerinckx, I. Kuzma, K. Van Nieuwenhuysen, H. J. Kim, and J. Poortmans, Thin Solid Films **511-512**, 533 (2006).
[3]M. L. Lee, G. Dezsi, and R. Venkatasubramanian, Thin Solid Films **518**, S76 (2010).
[4]M. Kolahdouz, A. A. Farniya, M. Östling, and H. H. Radamson, Solid-State Electron. **62**, 72 (2011).
[5]*Photonics and Electronics with Germanium*, edited by K. Wada and L. C. Kimerling (Weinheim, Wiley-VCH, 2015).
[6]U. Jain, S. C. Jain, J. Nijs, J. R. Willis, R. Bullough, R. P. Mertens, and R. Van Overstraeten, Solid-State Electron. **36**, 331 (1993).
[7]*Silicon-Germanium (SiGe) Nanostructures*, edited by Y. Shiraki and N. Usami (Woodhead, Cambridge, 2011).
[8]A. Alguno, N. Usami, T. Ujihara, K. Fujiwara, G. Sazaki, K. Nakajima, and Y. Shiraki, Appl. Phys. Lett. **83**, 1258 (2003).
[9]A. G. Aberle, S. Glunz, and W. Warta, J. Appl. Phys. **71**, 4422 (1992).
[10]D. Diouf, J. P. Kleider, T. Desrues, and P.-J. Ribeyron, Energy Procedia **2**, 59 (2010).
[11]R. Pandey and R. Chaujar, Sol. Energy **135**, 242 (2016).
[12]*Physics and Technology of Amorphous-Crystalline Heterostructure Silicon Solar Cells*, edited by W. G. J. H. M. van Sark, L. Korte, and F. Roca (Springer, Berlin, 2012).
[13]*Amorphous Silicon/Crystalline Silicon Heterojunction Solar Cells*, edited by W. R. Fahrner (Chemical Industry Press, Beijing; Springer, Berlin, 2013).
[14]S. Dauwe, J. Schmidt, and R. Hezel, in *29th IEEE Photovoltaic Specialists Conference* (2002).
[15]T. Krajangsang, S. Inthisang, J. Sritharathikhun, A. Hongsingthong, A. Limmanee, S. Kittisontirak, P. Chinnavornrungsee, R. Phatthanakun, and K. Sriprapha, Thin Solid Films **628**, 107 (2017).
[16]R. A. Street, *Hydrogenated Amorphous Silicon* (Cambridge University Press, Cambridge, 2005).
[17]Y. Yan, M. Page, T. H. Wang, M. M. Al-Jassim, H. M. Branz, and Q. Wang, Appl. Phys. Lett. **88**, 121925 (2006).
[18]M. Dürr and U. Höfer, Prog. Surf. Sci. **88**, 61 (2013).
[19]J. P. Seif, D. Menda, A. Descoeudres, L. Barraud, O. Özdemir, C. Ballif, and S. De Wolf, J. Appl. Phys. **120**, 054501 (2016).
[20]S. A. Hadi, P. Hashemi, A. Nayfeh, and J. Hoyt, ECS Trans. **41**, 3 (2011).
[21]E. Kadri, M. Krichen, and A. B. Arab, Opt. Quantum Electron. **48**, 305 (2016).
[22]E. Kadri, K. Dhahri, A. Zaafouri, M. Krichen, M. Rasheed, K. Khirouni, and R. Barillé, J. Alloys Compd. **705**, 708 (2017).
[23]P. Zaumseil, Y. Yamamoto, M. A. Schubert, T. Schroeder, and B. Tillack, Thin Solid Films **557**, 50 (2014).
[24]Y. Yamamoto, P. Zaumseil, T. Arguirov, M. Kittler, and B. Tillack, Solid-State Electron. **60**, 2 (2011).
[25]P. Zaumseil, Y. Yamamoto, A. Bauer, M. A. Schubert, and T. Schroeder, J. Appl. Phys. **109**, 023511 (2011).
[26]D. J. Eaglesham and M. Cerullo, Phys. Rev. Lett. **64**, 1943 (1990).
[27]A. A. Shklyaev, O. A. Shegai, Y. Nakamura, and M. Ichikawa, J. Appl. Phys. **115**, 203702 (2014).
[28]W. O. Filtvedt, A. Holt, P. A. Ramachandran, and M. C. Melaaen, Sol. Energy Mater. Sol. Cells **107**, 188 (2012).
[29]A. Podolian, V. Kozachenko, A. Nadtochiy, N. Borovoy, and O. Korotchenkov, J. Appl. Phys. **107**, 093706 (2010).
[30]A. Nadtochiy, A. Podolian, O. Korotchenkov, J. Schmid, E. Kancsar, and V. Schlosser, Phys. Status Solidi C **8**, 2927 (2011).
[31]P. H. Tan, K. Brunner, D. Bougeard, and G. Abstreiter, Phys. Rev. B **68**, 125302 (2003).
[32]M. I. Alonso, M. de la Calle, J. O. Ossó, M. Garriga, and A. R. Goñi, J. Appl. Phys. **98**, 033530 (2005).
[33]J. H. Lin, H. B. Yang, J. Qin, B. Zhang, Y. L. Fan, X. J. Yang, and Z. M. Jiang, J. Appl. Phys. **101**, 083528 (2007).
[34]E. O. Johnson, J. Appl. Phys. **28**, 1349 (1957).
[35]K. L. Luke and L. J. Cheng, J. Appl. Phys. **61**, 2282 (1987).
[36]*Handbook of Optical Constants of Solids*, edited by E. D. Palik (Academic, San Diego, 1998).
[37]E. Gaubas, E. Simoen, and J. Vanhellemont, ECS J. Solid State Sci. **5**, P3108 (2016).
[38]G. Pfister and H. Sher, Adv. Phys. **27**, 747 (1978).
[39]J. C. Phillips, Rep. Prog. Phys. **59**, 1133 (1996).
[40]*Nanostructured Semiconductors*, edited by P. Granitzer and K. Rumpf (CRC Press, Boca Raton, 2013).
[41]J. C. Phillips, J. Non Cryst. Solids **357**, 3853 (2011).
[42]V. Kuryliuk, O. Korotchenkov, and A. Cantarero, Phys. Rev. B **85**, 075406 (2012).
[43]J. Bian, L. Zhang, W. Guo, D. Wang, F. Meng, and Z. Liu, Appl. Phys. Express **7**, 065504 (2014).
[44]J. Mitchell, J. Appl. Phys. **114**, 193702 (2013).
[45]A. Metz *et al.*, Sol. Energy Mater Sol. Cells **120**, 417 (2014).
[46]N. Budini, P. A. Rinaldi, J. A. Schmidt, R. D. Arce, and R. H. Buitrago, Thin Solid Films **518**, 5349 (2010).
[47]F. Book, T. Wiedenmann, G. Schubert, H. Plagwitz, and G. Hahn, Energy Procedia **8**, 487 (2011).
[48]O. S. Panwar, R. A. Moore, N. S. J. Mitchell, H. S. Gamble, and B. M. Armstrong, Appl. Surf. Sci. **36**, 247 (1989).
[49]M. H. Brodsky, M. Cardona, and J. J. Cuomo, Phys. Rev. B **16**, 3556 (1977).
[50]R. J. Kobliska and S. A. Solin, Phys. Rev. B **8**, 3799 (1973).
[51]H. Richter, Z. P. Wang, and L. Ley, Solid State Commun. **39**, 625 (1981).
[52]M. Luysberg, P. Hapke, R. Carius, and F. Finger, Philos. Mag. A **75**, 31 (1997).
[53]M. N. Islam and S. Kumar, Appl. Phys. Lett. **78**, 715 (2001).
[54]C. Becker, F. Ruske, T. Sontheimer, B. Gorka, U. Bloeck, S. Gall, and B. Rech, J. Appl. Phys. **106**, 084506 (2009).
[55]A. Madan, Sol. Wind Technol. **5**, 473 (1988).
[56]R. J. Loveland, W. E. Spear, and A. Al-Sharbaty, J. Non Cryst. Solids **13**, 55 (1973/74).
[57]G. A. N. Connell and J. R. Pawlik, Phys. Rev. B **13**, 787 (1976).
[58]D. D. M. Wayner and R. A. Wolkow, J. Chem. Soc., Perkin Trans. **2**, 23 (2002).
[59]H. Heinz, C. Pramanik, O. Heinz, Y. Ding, R. K. Mishra, D. Marchon, R. J. Flatt, I. Estrela-Lopis, J. Llop, S. Moya, and R. F. Ziolo, Surf. Sci. Rep. **72**, 1 (2017).